

# Efficient dynamic fluid-structure computation for blade-mast interaction of a tidal turbine

Corentin Lothodé<sup>\*,\*\*,\*\*\*</sup>, Jules Poncin<sup>\*\*</sup>, Didier Lemosse<sup>\*\*\*</sup>, Emmanuel Pagnacco<sup>\*\*\*</sup>, Eduardo Souza de Cursi<sup>\*\*\*</sup>

\* LMRS, Université de Rouen

\*\* K-Epsilon

\*\*\* LMN, INSA Rouen

**Abstract-** In this article, we aim at providing results of fluid-structure interaction between water turbine blades and its mast. When the blade goes past the mast, a sudden pressure spike is recording, and the acceleration of the blade is recorded. Many results are provided, and two different structures are compared. At first, we validate our model against an experiment (Bahaj et al. [1]) as in [2]. This work is the direct continuation of [2] where many results of Computational Fluid Dynamics (CFD) were described. A methodology for estimating accurately the performance of a turbine for open water cases with CFD tools was outlined. The goal is now to validate those results for full cases (i.e. including the static parts) and including fluid-structure interaction effects. First, we validate the fluid only in dynamic mode. Then, several structures are setup by modifying the stiffness of the material and their behaviors are compared. We use K-FSI developed by K-Epsilon to solve the dynamic problem and the Quasi-Static Problem.

**Keywords-** water turbine, fluid-structure interaction, computational fluid dynamics

## I. INTRODUCTION

The experiment used is the one made by Bahaj et al. [1] was the first to be performed on tidal turbines. It contains many results for different pitch and is very useful to compare against. Though the experiment has a high blockage correction (up to 18%), it is well documented and provide much insight. Many people used this experiment to validate codes, Blade Element Momentum Theory (BEMT) for example in [3]. Other experiments exist today but will not be used in this paper (Ifremer [4], Liverpool [5,6], Manchester [7]). BEMT is a good approach to assess the performance of one turbine, but it fails to perform for multiple turbines. To avoid this problem, other approaches has been developed such as the Vortex Lattice Method (VLM) in [8]. Their focus is the wake of the turbine to study the interaction between two or more turbines [9]. Their results are good until stall which is expected since their method force the flow to be attached until the trailing edge. Later [10] included turbulence.

Attempts to use CFD on wind or tidal has been performed in the past. To avoid too much computational efforts, many authors modelled the behaviour of the turbine instead of resolving the full geometry. For instance, [11] has used Large Eddy Simulation (LES) with the turbine replaced by an approximated model of a concentrated drag force to study the wake development. Also using an approximated model for the turbine, [12] performed a LES computation using an actuator disk. Fully resolved blade geometry CFD computations are computationally expensive but can give many more insight about the flow behaviour and force distribution along the blade. [13] compared  $k-\omega$  SST, Launder-Reece-Rodi turbulence model (LLR) and LES on the  $20^\circ$  pitch angle case of [1] as an unsteady simulation, including the mast and a simplified geometry of the cavitation tunnel. The work this paper is based on, [2], did the fully resolved geometry CFD computations with  $k-\omega$  SST on all angles using Multiple Rotating Frame (MRF) method.

Fluid-Structure Interaction (FSI) is widely used for the design of wind turbines, but most of the time it is not using CFD. For example, the industry standard Bladed is used, or the opensource FAST [14] are both using BEM method to compute the fluid loads (with additional models to predict dynamic loads). It is with the work of [15] and [16] that the first dynamic FSI computations were performed on wind turbines. Yet, it is so computationally intensive that very few people are trying to perform this kind of computations. Concerning water turbine or tidal turbines, no dynamic FSI computations were performed to the author's knowledge.

The tools used in this paper are described in detail in [17] and [18]. The fluid solver is ISIS-CFD. It is included in FINE<sup>TM</sup>/Marine and is developed by the METHRIC team of LHEEA laboratory and commercialized by NUMECA International. It solves the Reynolds-Averaged Navier-Stokes Equations in a strongly conservative way. It is based on the finite volume method and can work on structured or unstructured meshes with arbitrary polyhedrons. The equations are formulated according to the Arbitrary Lagrangian Eulerian paradigm and therefore can easily work with mesh deformations. Several turbulence models are implemented in ISIS-CFD. In this study, we used the SST-

$k-\omega$  model. The mesh is generated with Hexpress™ (which is part of FINE™/Marine) with an octree method. The solver ARA is developed by the company K-Epsilon. The code was initially aimed at simulating the dynamic behavior of sailboat rigs: sails, mast and cables. A non-linear finite element method with a large deformation formulation is implemented. While numerous element types have been implemented in the structural code, in the present study, only beam elements are used. These elements are Timoshenko elements, with the hypothesis of small deformations. Each beam element is defined thanks to two points (for position) and two quaternions (for the tangent directions). The fluid structure interface is entirely defined by the fluid faces. Each fluid node is projected onto the nearest beam elements to get a parameterized position of the projected point as well as a vector linked to the local frame of the beam. When the beam is deformed, the 3D deformation of the neutral axis is computed with the variation of the local frame from one end to the other end of the beam. The local frame evolves smoothly according to a cubic spline law. Therefore, the new fluid node position is computed from the new position of the neutral axis and its local frame. Following the interface deformation, the whole mesh of the fluid domain needs to be deformed. This deformation occurs at each coupling iteration. The number of call to this procedure being non-negligible, the mesh deformation needs to be fast. To do this, a new method was developed that propagates the deformation state to the fluid mesh.

## II. DYNAMIC FLUID VALIDATIONS

### A. Description of the case

The experiment is fully described in [1]. The tests were carried out in a cavitation tunnel at Southampton Institute (see Figure 1). The rotor diameter of the turbine is 800mm. It was chosen as a compromise between maximizing Reynolds number and not inducing too much tunnel blockage correction. The blockage correction is based on an actuator disk model of the flow through the turbine in which the flow is presumed to be uniform across any cross-section of the stream tube enclosing the turbine disc [19]. For example, with a single rotor and a thrust coefficient of 0.8, the corrections amounted up to 18% decrease in power coefficient and 11% decrease in thrust coefficient for the cavitation tunnel and up to 8% and 5% decrease, respectively, for the towing tank.



**Figure 1:** Photo of the experiment (from [1])

The blades are made from the NACA 63-8xx series (see Figure 2). The distribution of pitch and thickness can be found in [1] and [2]. We kept the values used in [1] meaning that the pitch distribution is in fact the pitch of the element at radius 80mm (15° means taking the blade as the original blade pitch, 20° means imposing 5° pitch to the blade). Many tests were performed: varying the tip immersion, the blade pitch angle and yaw angle. In this paper, only the angle 20° is considered. The flow speed is 1.73 m/s.

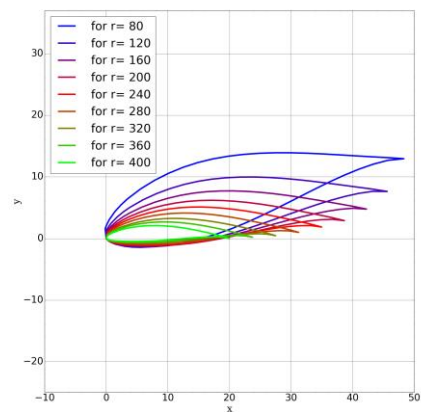


**Figure 2:** Overview of all sections and pitch (for 20°) (r in mm)

### B. Comparison between MRF and dynamic rotation.

As in [2], the fluid domain is decomposed in two parts. A part that contains the bigger domain, supposedly the size of the cavitation tunnel. A smaller domain, cylindrical, represent the domain in rotation. It includes the hub part that is rotating and the blades. The two domains are shown in Figure 3. The inner domain can rotate inside the outer domain. The two domains are linked through a sliding interface.

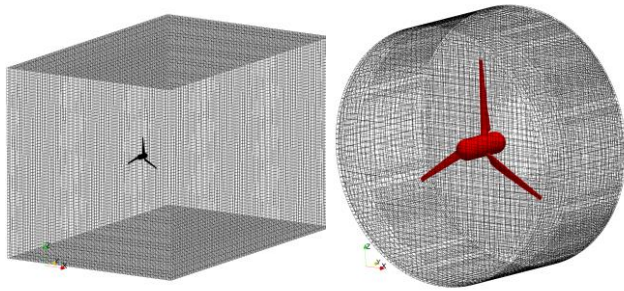


Figure 3: Overview of the computational domains

We describe two ways of computing the performance of water turbine. We can use either MRF computations or dynamic computations. MRF stands for Multiple Reference Frame. In this method, we exploit the ALE (Arbitrary Lagrangian Eulerian) capability of ISIS. All the meshes components are fixed, but an additional mesh velocity is given to the rotating part.

The dynamic computations are moving the mesh at each time step. A new position of the points is given, and a speed is computed according to this movement, using Backward Differentiation Formula of order 2. Here, we want to compute the open water performance. In the end, we want to study a stationary problem, which is well adapted to MRF computations. The final goal of this paper being the computation of a dynamic fluid-structure interaction problem, we need to see if the results are similar and well adapted and that the parameters are well chosen. In the case of a MRF computation, the best practices advice to use a time step of a 1/20<sup>th</sup> of a rotation. In the case of a dynamic computation, the best practices are to use a time step of 1/100<sup>th</sup> of a rotation.

Ct stands for coefficient of thrust and is a nondimensionalized number related to the thrust of a turbine. It is equal to the force in the flow direction divided by  $\rho V \pi r^2$ . Cp stands for coefficient of power and is a nondimensionalized number related to the torque of a turbine. It is equal to the torque times the rotation speed divided by  $\rho V \pi r^3$ .  $\rho$  is the volumic mass of the fluid (here 998.3 kg/m<sup>3</sup>).  $r$  is the radius of the turbine (here 0.4m). The fluid velocity in this case is 1.73 m/s<sup>2</sup>. TSR stands for Tip Speed Ratio and is the ratio between the speed of the tip of the blade and the flow velocity.

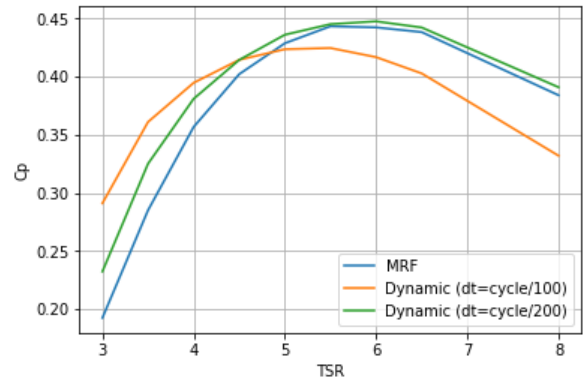
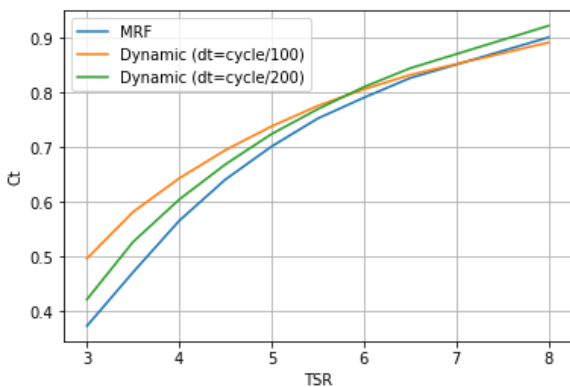


Figure 4: Comparison between MRF and Dynamic method

Performing a first set of computation using the best practices, the first results obtained were really different (as seen in Figure 4). A second set of dynamic computations was launched using a time step of 1/200<sup>th</sup> of a rotation, and the results were a lot more in agreement to each other. A difference can exist because of the dynamic behavior of the flow that is described with a better accuracy in the case of a dynamic computation. In addition, the wake of the rotor, in the bigger computational domain, is very different when using dynamic computations. In conclusion, the use of a time step below a 1/200<sup>th</sup> of a rotation is acceptable. It is difficult to accept much less of this value, since the computational effort is getting bigger with a lower time step.

### III. FLUID-STRUCTURE COMPUTATIONS

#### A. Quasi-static computation

The structures properties were obtained base on the same kind of structure that can be done for wind turbines. A box at the largest part of the profile is reinforced (see Figure 5). We consider rigid the root of the blade (between 0.04 and 0.08, in red in the figure). The obtained properties are shown in the Figure 5. For the structure labeled as E4, we used a Young modulus of 69GPa, corresponding to aluminum. We introduce two other Young moduli: E2=E4/2 and E1=E4/4. The results using the module Young labeled E4 are referred as E4. We do the same for E2 and E1.

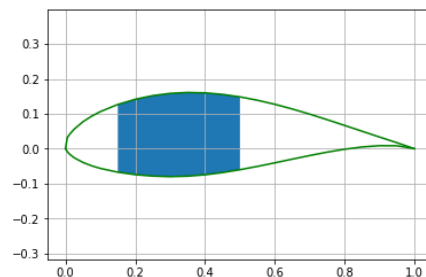
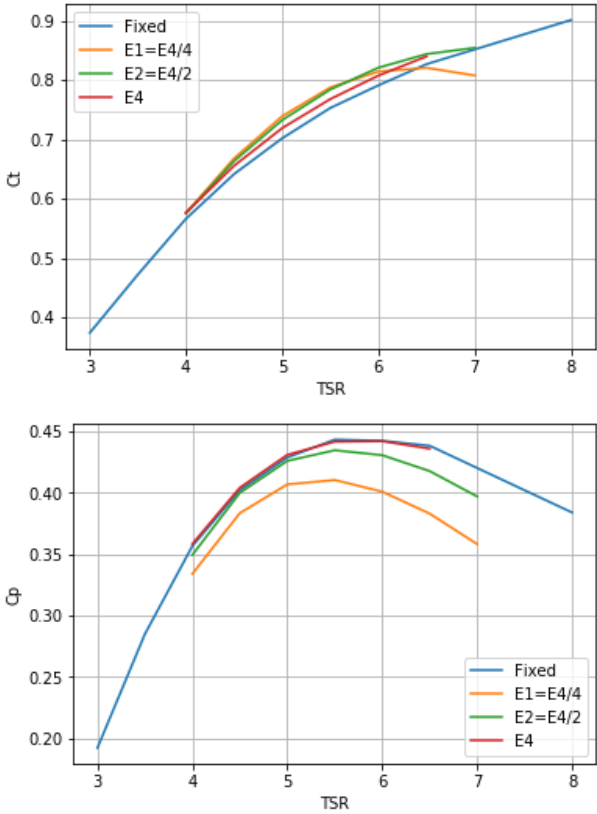


Figure 5: The box reinforced in blue for section at r=80mm

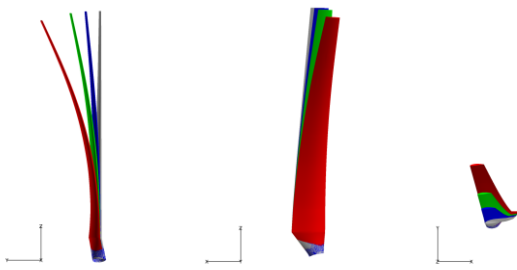
The performance curves were redone using the different structures, using quasi-static computations (i.e. only looking at the steady phenomenon). Quasi-static computations consist of running a long steady fluid computation. After each

convergence of the fluid forces, the structure is released using a steady state scheme. After few iterations, the forces between the structure and the fluid are in equilibrium.



**Figure 6:** Performance curves for different structural properties.

In Figure 6, we can see that the results between the fixed computation and E4 are close. The  $C_t$  is a little bit superior, but the  $C_p$  is quasi identical. E2 and E4 are also showing an increasing  $C_t$ , but there is a decay for high TSR, because the blade aligns itself with the flow.  $C_p$  performances are getting worse and worse with the decreasing stiffness, for the same reason.



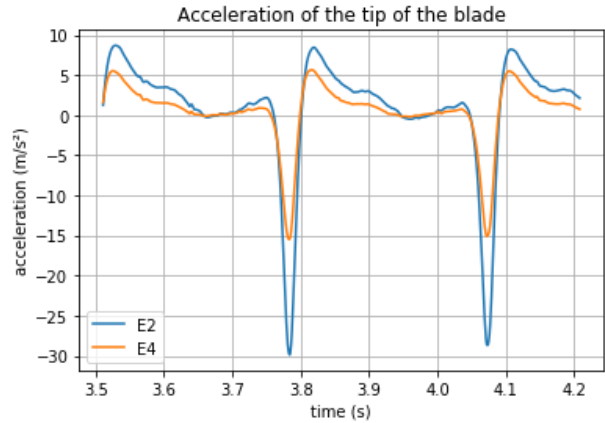
**Figure 7:** Different views of the deformed blades (grey: fixed, blue: E4, green: E2, red: E1)

Figure 7 shows the deformed blade for the different Young moduli at TSR5. E1 has the biggest deflection, and is quite unrealistic. The deflection occurs both in the flow direction and the rotation direction because of the traction.

**B. Blade-mast dynamic interaction with FSI**

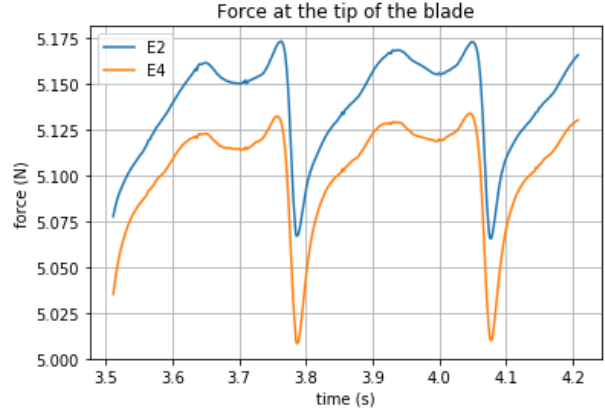
A mast is added to the computation domain. The mast is considered rigid. The hub now has two parts, one that is fixed and linked to the mast, and a part that is rotating with the blades.

We chose to consider E4 and E2 only, because E1 showed very poor results and was considered unrealistic. We used a time step of  $10^{-3}$ s, which is lower than a  $1/200^{\text{th}}$  of a rotation. The water turbine is rotating at 21.625 rad/s which corresponds to TSR5. The frequency of the blade passage in front of the mast is 3.44Hz. We record the position and efforts on all structural points of the blade.



**Figure 8:** Acceleration of the tip of the blade (in  $m/s^2$ ).

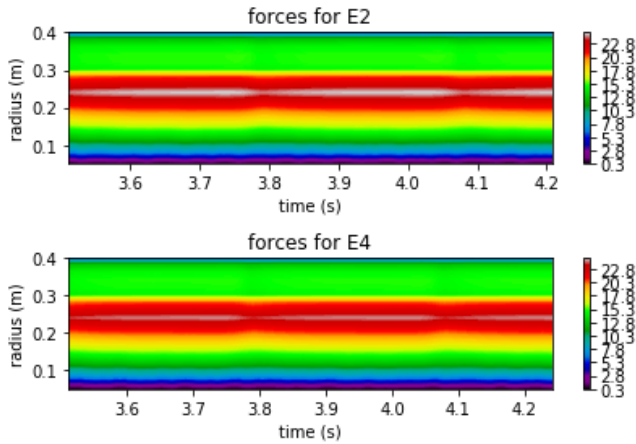
Acceleration at the tip of the blade is shown in Figure 8. The start of the graph shows the recovery after the shock. At  $t=3.78$ , the blade arrives near the mast. The acceleration reaches  $30m/s^2$  for E2 and  $15m/s^2$  for E4. The recovery starts with an acceleration peaking at  $8m/s^2$  for E2 and  $6m/s^2$  for E4 at  $t=3.82s$  for E2 and  $3.81s$  for E4. The time for recovery (acceleration of  $\sim 0m/s$ ) is approximately the same and take  $\sim 0.17s$ . A cycle takes  $0,29s$  at TSR5. The first acceleration and its recovery takes  $\sim 60\%$  of a cycle. For larger TSR, this would be even more noticeable.



**Figure 9:** Force at the tip of the blade (in N).

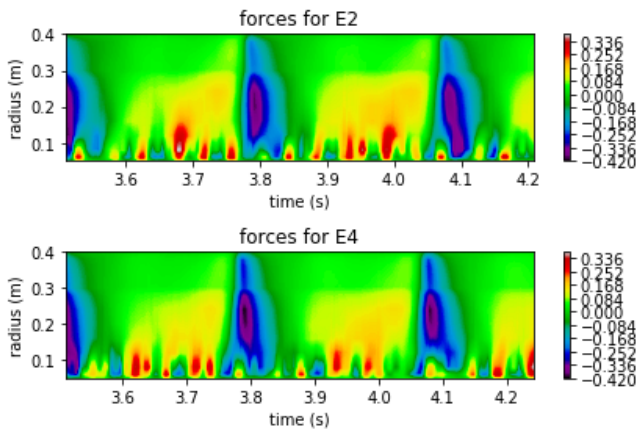
Figure 9 shows the efforts at the tip of the blade. The difference between E2 and E4 is 50N at  $t=3.75$  (1% of the

efforts) and reaches 70N at t=3.78s (1.4%). The efforts are showing a very close behavior between the two stiffness.



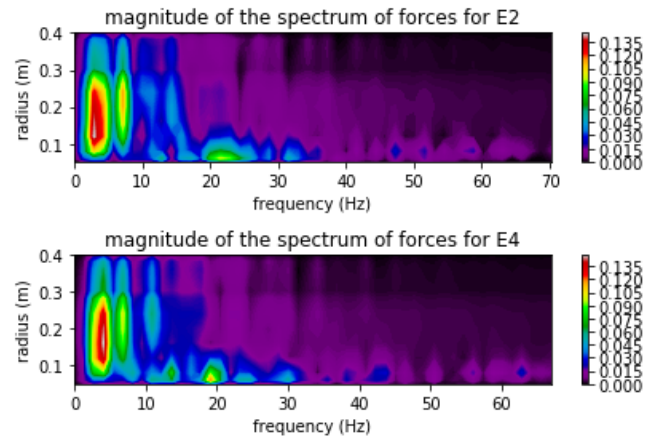
**Figure 10:** Force on the blade according to time (in N).

Figure 10 shows the absolute efforts acting on each structural node of the blade. The loading is the biggest at the center of the beam (23N at r=0.25m) and the lowest at the root of the blade (0.3N). Furthermore, the loading extends further on the upper part of the blade than on the lower part of the blade. On the upper part of the beam the loading is almost constant and approximately 15N (from r=0.3m to r=0.38m) and on the lower part of the beam it evolves almost linearly between the maximum value of 23N to 0.3N at the root of the blade. It is difficult to see a transient behavior. Between E2 and E4, it is also very difficult to notice a difference.



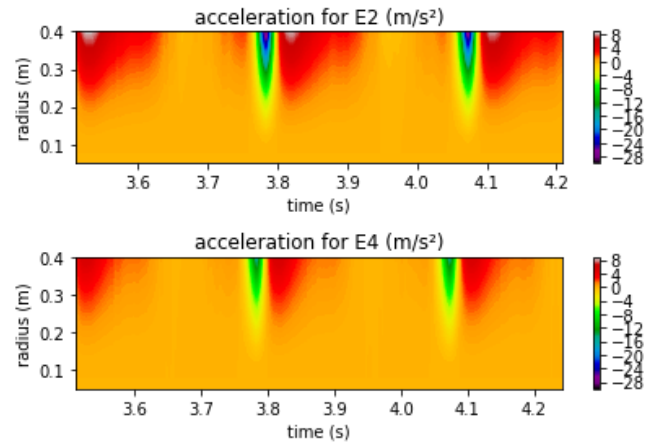
**Figure 11:** Difference between current force and mean force for each structural node of the blade according to time (in N).

Figure 11 shows the difference between the current force and the beam force for each structural nodes of the blade according to time. With this postprocess, it is much easier to see the transient behavior. At the part above r=0.1m, there is a negative spike in forces just at the passage of the mast. It is then recovered with a more continuous positive pressure. The negative spike occurs on the whole blade, especially for E4, the upper part for E2 being less spiky. There are very fluctuating efforts at the root of the blade.



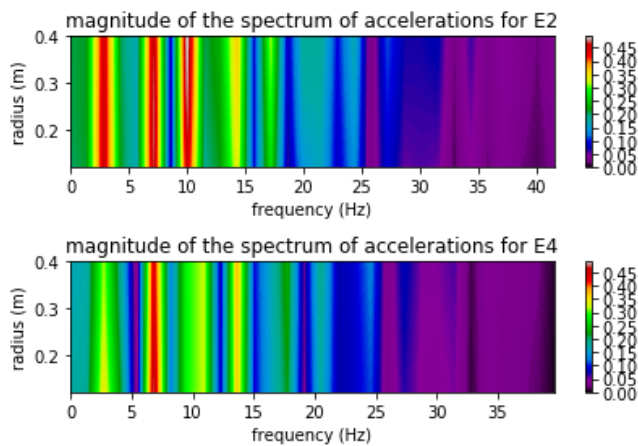
**Figure 10:** Fourier transform of the forces (magnitude).

Figure 10 shows the forces in the frequency space. For E2 and E4 the frequency corresponding to the rotation frequency are highly excited as expected. The second mode (~7Hz) is higher for E2 than for E4. It is the contrary for the third mode (~10.3Hz). The fourth mode (~14Hz) is existent in E2 but almost not for E4. At the root of the blades, the frequency we can see are related to the vortex advected in the flow.



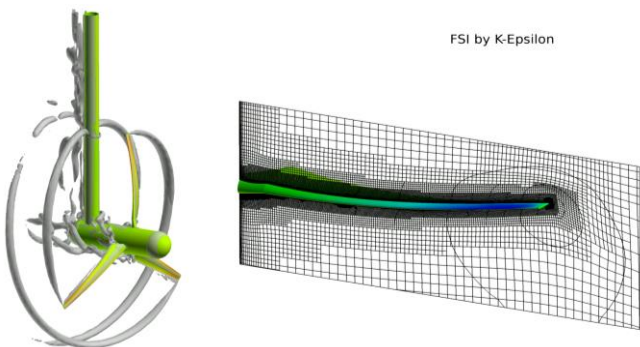
**Figure 11:** Acceleration of each structural node of the blade according to time (in m/s<sup>2</sup>).

Figure 11 shows the acceleration of each structural node of the blade. The acceleration is the biggest at the tip of the blade, as one should expect. As seen before, the acceleration peak is half the magnitude for E4 compared to E2. The most interesting feature is the positive acceleration after the peak, called here recovery, which is shorter in duration when the stiffness is higher. For E2, the acceleration is nonnegligible for a large portion of the cycle, when for E4 it is concerning less than half of the cycle.



**Figure 12:** Fourier transform of the acceleration (scaled radius by radius).

Figure 12 shows the Fourier transform of the acceleration for each structural node of the blade. It is scaled radius by radius to show which mode is excited for each configuration. For E2 the first mode, which is the frequency of rotation 3.44Hz, is highly excited, when for E4 it is much less the case. Second mode (~7Hz) is the principal mode to be excited for E4 and is also excited for E2. Third mode (~10Hz) is highly excited for E2 but not for E4. Fourth mode (~14Hz) is more excited for E4 than E2. There is not a huge difference in spectrum for between the tip and the root except for very high frequencies.



**Figure 12:** Instant view of the simulation showing the iso-value of the Q criterion.

The Figure 12 is showing the tip vortices thanks to the Q criterion (TSR5 and E2). We can see the deflection with the deformed mesh on the right side of the Figure. The vortices at the root of the blades are also showing.

#### IV. CONCLUSION

A dynamic methodology was developed to simulate fluid only computation and was validated against older results from [2]. Three different structures were setup and simulated using quasi-static fluid-structure computations showing interesting behavior at high TSR. The most flexible structure seems not suitable for production. The two other structures were setup with a mast and the dynamic displacement and forces recorded for comparison. Different behaviors were highlighted. For future work, it would be interesting to

compare against existing experimental data. Quasi-static optimization of the structure would be insightful.

#### APPENDIX

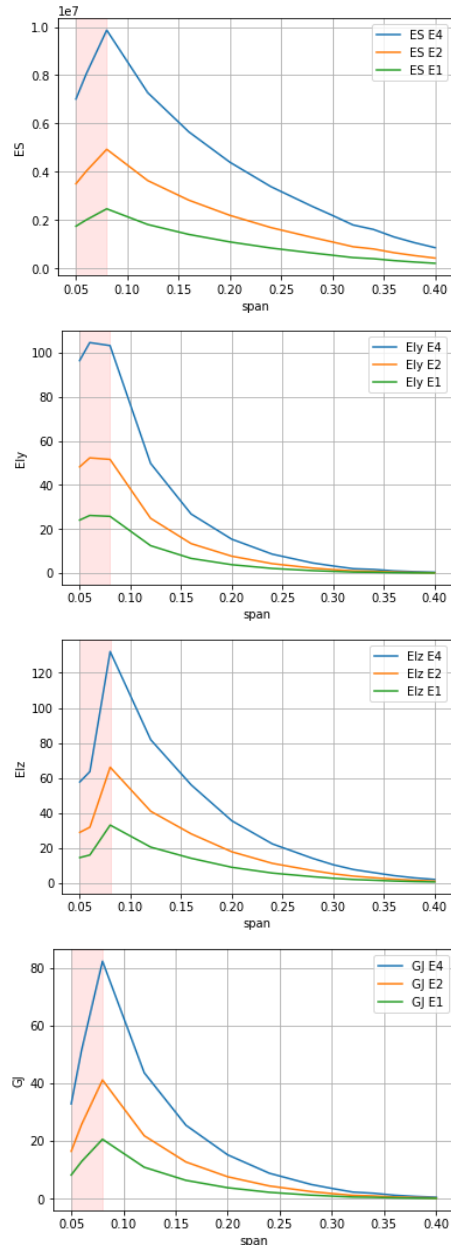


**Figure A :** Structural properties of the beam along the span of the blade.

#### ACKNOWLEDGMENT

This work was initially funded by K-Epsilon and the ANRT through a CIFRE PhD Scholarship and a partnership with LMN of INSA Rouen. K-Epsilon is still supporting the project through a partnership with the LMRS – CNRS. We are thankful for the computing support provided by the CRIANN. We want to thank NUMECA International for the R&D license.

## REFERENCES

- [1] AS Bahaj, AF Molland, JR Chaplin, and WMJ Batten. Power and thrust measurements of marine current turbines under various hydrodynamic flow conditions in a cavitation tunnel and a towing tank. *Renewable energy*, 32(3):407–426, 2007.
- [2] C Lothodé, D Lemosse, E Pagnacco, E Souza, A Hugues, Y Roux. Simulation validation of a tidal turbine: comparison to Southampton’s experiment. NUTTS 2017.
- [3] WMJ Batten, AS Bahaj, AF Molland, JR Chaplin, Sustainable Energy Research Group, et al. Experimentally validated numerical method for the hydrodynamic design of horizontal axis tidal turbines. *Ocean Engineering*, 34(7):1013–1020, 2007.
- [4] P Mycek, B Gaurier, G Germain, G Pinon, and E Rivoalen. Experimental study of the turbulence intensity effects on marine current turbines behaviour. part i: One single turbine. *Renewable Energy*, 66:729–746, 2014.
- [5] SC Tedds, Ieuan Owen, and RJ Poole. Near-wake characteristics of a model horizontal axis tidal stream turbine. *Renewable Energy*, 63:222–235, 2014.
- [6] TA de Jesus Henriques, SC Tedds, A Botsari, G Najafian, TS Hedges, CJ Sutcliffe, Ieuan Owen, and RJ Poole. The effects of wave–current interaction on the performance of a model horizontal axis tidal turbine. *International Journal of Marine Energy*, 8:17–35, 2014.
- [7] E Fernandez-Rodriguez, TJ Stallard, and PK Stansby. Experimental study of extreme thrust on a tidal stream rotor due to turbulent flow and with opposing waves. *Journal of Fluids and Structures*, 51:354–361, 2014.
- [8] G Pinon, P Mycek, G Germain, and E Rivoalen. Numerical simulation of the wake of marine current turbines with a particle method. *Renewable Energy*, 46:111–126, 2012.
- [9] P Mycek, B Gaurier, G Germain, C Lothode, G Pinon, and E Rivoalen. Numerical and experimental characterisation of interactions between two marine current turbines. *Revue Paralia*, 6, 2013.
- [10] C Carlier, G Pinon, B Gaurier, G Germain, and E Rivoalen. Numerical and experimental study of elementary interactions in marine current turbines array. In *11th European Wave and Tidal Energy Conference (EWTEC)*, 2015.
- [11] A Jimenez, A Crespo, E Migoya, and J Garcia. Advances in large-eddy simulation of a wind turbine wake. In *Journal of Physics: Conference Series*, volume 75, page 012041. IOP Publishing, 2007.
- [12] M Calaf, C Meneveau, and J Meyers. Large eddy simulation study of fully developed wind-turbine array boundary layers. *Physics of Fluids (1994-present)*, 22(1):015110, 2010.
- [13] I Afgan, J McNaughton, S Rolfo, DD Apsley, T Stallard, and P Stansby. Turbulent flow and loading on a tidal stream turbine by les and rans. *International Journal of Heat and Fluid Flow*, 43:96–108, 2013.
- [14] J Jonkman. NWTC design codes (FAST). NWTC Design Codes (FAST), NREL, Boulder, CO, 2010.
- [15] Y Bazilevs, M-C Hsu, J Kiendl, R Wüchner, K-U Bletzinger, 3D simulation of wind turbine rotors at full scale. Part II: Fluid–structure interaction modeling with composite blades, *Int. J. Numer. Methods Fluids* 65 (2011) 236–253.
- [16] K. Takizawa, B. Henicke, D. Montes, T.E. Tezduyar, M.-C. Hsu, Y. Bazilevs, Numerical-performance studies for the stabilized space-time computation of wind-turbine rotor aerodynamics, *Comput. Mech.* 48 (2011) 647–657
- [17] C Lothodé, M Durand, Y Roux, A Leroyer, M Visonneau, L Dorez. *Dynamic Fluid Structure Interaction of a Foil. Innov’ Sail*, 2013.
- [18] M Durand, *Interaction fluide-structure souple et légère, applications aux voiliers*, Ph.D. thesis, Ecole Centrale Nantes, 2012.
- [19] MJ Barnsley and JF Wellicome. Final report on the 2nd phase of development and testing of a horizontal axis wind turbine test rig for the investigation of stall regulation aerodynamics. carried out under etsuagreement e. carried out under ETSU Agreement E. A, 5, 1990.

## AUTHORS

**Corentin Lothodé** – Corentin Lothodé, Research Engineer, LMRS Université de Rouen, corentin.lothode@univ-rouen.fr.

**Jules Poncin** – Jules Poncin, Engineer, K-Epsilon, jules@k-epsilon.com.

**Didier Lemosse** – Didier Lemosse, Associate Professor, INSA Rouen, didier.lemosse@insa-rouen.fr.

**Emmanuel Pagnacco** – Emmanuel Pagnacco, Associate Professor, INSA Rouen, emmanuel.pagnacco@insa-rouen.fr.

**Eduardo Souza de Cursi** – Eduardo Souza de Cursi, Professor, INSA Rouen, eduardo.souza@insa-rouen.fr.

**Correspondence Author** – Corentin Lothodé, corentin.lothode@univ-rouen.fr, 02 32 95 52 68